

Article

Effect of Dolomite Addition on the Structure and Properties of Multicomponent Amphibolite Glasses

Adrian Nowak ¹, Malgorzata Lubas ¹, Jaroslaw Jan Jasinski ^{2,*}, Magdalena Szumera ³, Renata Caban ¹, Jozef Iwaszko ¹ and Kamila Koza ¹

¹ Department of Materials Engineering, Czestochowa University of Technology, Armii Krajowej 19, 42-200 Czestochowa, Poland; adrian.nowak@pcz.pl (A.N.); malgorzata.lubas@pcz.pl (M.L.); renata.caban@pcz.pl (R.C.); jozef.iwaszko@pcz.pl (J.I.); kama130395@interia.pl (K.K.)

² Materials Research Laboratory, National Centre for Nuclear Research, 05-400 Otwock, Poland

³ Faculty of Materials Science and Ceramics, AGH University of Science and Technology, Al. Mickiewicza 30, 30-059 Cracow, Poland; mszumera@agh.edu.pl

* Correspondence: jaroslaw.jasinski@ncbj.gov.pl; Tel.: +48-222-731-062

Abstract: The structure and properties of the glass can be modified by introducing appropriate additives. Dolomite is one of the primary raw materials modifying the properties of glass, in which the essential component is calcium-magnesium double carbonate $\text{CaCO}_3 \cdot \text{MgCO}_3$. The paper presents the research results on glasses obtained by smelting pure amphibolite and amphibolite modified with 10 and 20% dolomite additives. The raw material used was mined in the Poland region of Lower Silesia. The glass melting process was carried out in an electric furnace at 1450 °C for 2 h. The structure and properties of the glasses and crystallization products were determined by Differential Scanning Calorimetry (DSC), X-ray Diffraction (XRD), Fourier Transform Infrared Spectroscopy (FTIR) and Scanning Electron Microscopy—Energy Dispersive Spectroscopy (SEM-EDS). Viscosity and Vickers microhardness were also measured. It was found that the modification of amphibolite glass by adding dolomite affects the glasses' properties and structure. The research results determined the effect of dolomite addition on the properties of alumino-silicate glasses in terms of the mineral fibre products used in the construction industry.

Keywords: structure glass; amphibolite glass; dolomite addition; crystallization; glass-ceramic materials; differential scanning calorimetry DSC



Citation: Nowak, A.; Lubas, M.; Jasinski, J.J.; Szumera, M.; Caban, R.; Iwaszko, J.; Koza, K. Effect of Dolomite Addition on the Structure and Properties of Multicomponent Amphibolite Glasses. *Materials* **2022**, *15*, 4870. <https://doi.org/10.3390/ma15144870>

Academic Editors: Robert F. Tournier and Michael I. Ojovan

Received: 25 May 2022

Accepted: 11 July 2022

Published: 13 July 2022

Publisher's Note: MDPI stays neutral with regard to jurisdictional claims in published maps and institutional affiliations.



Copyright: © 2022 by the authors. Licensee MDPI, Basel, Switzerland. This article is an open access article distributed under the terms and conditions of the Creative Commons Attribution (CC BY) license (<https://creativecommons.org/licenses/by/4.0/>).

1. Introduction

Rapid economic and technological development drives the search for new solutions and raw materials in the glass and construction industries. $\text{CaO-MgO-Al}_2\text{O}_3\text{-SiO}_2$ (CMAS) glasses are among the most essential glass systems with broad applications in these industrial areas due to their excellent chemical and mechanical properties. They are used to produce glass-ceramic materials and glass and mineral fibres [1–5]. These glasses can be obtained from appropriately composed glass sets based mainly on mineral raw materials, e.g., basalt, as in the case of mineral wool production, which is widely used as thermal and acoustic insulation material in heat treatment furnaces, thermal pipelines, construction walls, etc. [6–8]. More than 55% of insulating materials work at temperatures up to 200 °C, about 25% in the range 180–400 °C, 5% in the range 400–600 °C, and only 0.1% are installed in conditions where temperature values exceed 600 °C [9–11]. The significant disadvantage of mineral fibre wool is the loss of rigidity of the structure. It results, among others, from the usage as a binding agent of synthetic material-phenol-formaldehyde resin with a low range of working temperature (max. 250 °C) [12]. From the construction industry practice, it is known that temperature, moisture and frost can significantly affect the thermal and mechanical properties of insulation materials used in roof panels, facades and foundations [13]. Therefore, producing of a lightweight, non-combustible,

weather-resistant, and environmentally friendly insulating material operating at temperatures above 600 °C is a very important subject in the field. Drozdyuk et al. presented the possibility of using bentonite clay as high plasticity binding agent. This material is a layered silicate-montmorillonite group, and its solid mineral particles in suspension contain 63% saponite, 10% quartz, 10% dolomite and other minerals: chlorite, hematite, calcite, apatite, not exceeding 2–3%. Based on the research, the authors showed that the binder makes it possible to produce a thermal insulation material on an industrial scale without changing the production technology of conventional mineral fibre wool. Moreover, the method of applying clay as a binder was successfully implemented in the production line at the Insulation Plant “Zavod Izolatsi” Irpen, Ukraine [14]. The second important factor affecting fibre durability is moisture content. Vrana and Gudmundsson studied the effect of moisture on the properties of cellulose fibres and stone wool over several days [15,16]. They showed that there were slight changes in the water vapour permeability of the fibres. On the other hand, Jerman et al. observed that the thermal conductivity of mineral fibre wool increases rapidly at elevated humidity, from 0.041 W/mK under dry conditions to 0.900 W/mK under saturated conditions [17]. Additionally, Vrana and Bjork studied frost’s effect on different densities of mineral wool. Their results showed that the moisture content was 2.5 or 3 times higher than expected in lower-density insulation materials [18].

In recent years, continuous basalt fibres (CBFs) have also received increasing attention in science and industrial applications of fibre materials [19]. Compared to glass fibre production, the modulus and strength values for high-grade basalt fibres are between E and S2 glass fibres with excellent performance versus cost. Basalt fibres respond to market demand and rising costs in industries that widely use glass fibres e.g., aerospace, automotive and construction [20]. The thermal, chemical, and tribological resistance and insulating properties of basalt fibres can also be a significant added value to the manufacturing of composite materials. The choice of basalt rock as raw material for fibre production is mainly determined by the chemical composition of the fibres, which is similar to that of glass fibres. The optimum SiO₂ content for CBF production is above 46%. Higher contents improve the fibres’ spinning process and mechanical properties, as does the alumina content [21,22]. The main difference in chemical composition between basalt and glass fibres is the high percentage of iron content in CBF. The proportion of iron oxides Fe₂O₃ and FeO influence temperature forming, crystallization ability, and mechanical properties of CBF [23–25]. Additional oxides typically present in CBF are CaO, MgO, Na₂O, K₂O, and TiO₂. Bauer et al. investigated basalt fibres’ structure versus property relationships for high-performance applications. They showed that despite using natural basalt rock as raw material, the measured variation in fibre chemistry between batches was less than 1% of the total standard deviation [26]. As mentioned, basalt fibre’s mechanical properties range between E and S2 glass. For the basalt fibres, an inverse tendency of decreasing strength and elongation to break at growing mean fibre diameters is observed and relates to the size effect. In basalt and glass fibres, the mechanical performance increases with higher amounts of silica, alumina, and magnesia (glass formers).

Besides the mentioned basalt, alternative raw materials such as gabbro are also used for insulating materials (mineral wool, CBF) production [27,28]. Therefore, research to find new natural raw materials that meet the criteria for mineral fibre production is still carried out. Considering as interesting raw material for such applications are amphibolites. These are metamorphic rocks whose main components are amphiboles (hornblende, gedrite, cummingtonite) and plagioclase. Besides, the minerals include quartz, epidote, zoisite, garnets, biotite, cordierite, andalusite, sillimanite, tourmalines, titanite, ilmenite, and pyroxenes. Currently, these raw materials are used mainly as broken aggregate in road and railroad construction, as cement additives, or as mineral fertilizer [29–31]. However, appropriately composed amphibolite glasses possess suitable properties (crystallization ability, viscosity, acid modulus) to produce glassy insulation materials. This has been studied by Operta and Lampropoulou [32,33]. They showed that the chemical and major mineralogical composition, the heterogeneous characteristics of textures as well as the frequent presence

of phyllosilicates due to the weathering of the plutonic studied samples, are expected to contribute to easier grinding and melting of rocks under industrial conditions and to produce new light coloured and competitive stone wool product. Such research confirms that this is a developmental topic. Nevertheless, the high level of industry interest in the selection of raw materials (amphibolites) and parameters for obtaining fibres evidenced mainly by patents results in a lack of scientific publications in this field [34,35]. However, it should be mentioned that amphibolite raw materials often require modification due to their chemical and mineralogical composition. One of the basic raw materials modifying the properties of amphibolite glass is dolomite, whose primary component is a double calcium-magnesium carbonate $\text{CaCO}_3 \cdot \text{MgCO}_3$ [36]. By introducing dolomite into the glassmaking set, we introduce calcium and magnesium oxides, which influence the thermal stability of glass, its liquidity temperature, and viscosity. Therefore, a properly selected raw material composition, i.e., the proportion of additives and the chemical composition of the set, highly determines the properties and the application of the finished product. In addition, the so-called intrinsic factors, which include viscosity, surface tension, and melt stability, are also important [37,38]. This paper describes the influence of dolomite addition on the structure and properties of amphibolite glasses after melting and directed crystallization in terms of the mineral fibre production used in insulation materials e.g., mineral wool.

2. Materials and Methods

Natural raw materials from the Lower Silesia region of Poland: amphibolite and dolomite, shown in Figure 1, were used in the study. The chemical composition of the raw materials was analyzed by X-ray fluorescence (XRF) spectroscopy using an Axios mAX WDXRF spectrometer with a 4 kW Rh lamp manufactured by PANalytical, Malvern, United Kingdom (Table 1).



Figure 1. Natural raw materials from the Lower Silesia region of Poland used to melt glasses, (a) amphibolite, (b) dolomite.

Table 1. Chemical composition analysis of raw materials used to melt glasses [wt.%].

Raw Material	Composition, [wt.%]												
	Na ₂ O	MgO	Al ₂ O ₃	SiO ₂	P ₂ O ₅	SO ₃	K ₂ O	CaO	TiO ₂	MnO	Fe ₂ O ₃	ZrO ₂	PbO
Amphibolite	5.41	4.78	14.1	54.6	<0.10	<0.1	0.22	6.08	1.08	0.25	10.3	<0.1	-
Dolomite	0.37	36.93	1.37	3.27	0.06	0.08	0.19	59.34	0.04	0.19	0.83	0.26	0.04

Three glassmaking sets were prepared for tests and characterization of the selected raw materials, which contained different proportions of amphibolite and dolomite additions: Set 1*—100 wt.% amphibolite, Set 2*—90 wt.% amphibolite/10 wt.% dolomite, Set 3*—80 wt.% amphibolite/20 wt.% dolomite. The prepared, crumbled, homogenized sets were then placed in alundum crucibles and melted in an electric chamber furnace. The samples were melted at a maximum temperature of 1450 °C for 2 h so that the resulting melt was bubble-free and highly homogeneous. The melt was then cast directly onto a steel plate to ensure a maximum cooling rate. X-ray fluorescence (XRF) spectroscopy determined the chemical composition of the melted samples, as in the case of raw materials. Phase and structural studies were conducted using XRD and FTIR spectroscopic analysis. The X-ray analysis was carried out on a SEIFERT XRD-3003 T-T XRD Eigenmann GmbH, Schnaittach, Germany; X-ray diffractometer with a Co lamp with a wavelength of $\lambda_{\text{Co}} = 0.17902 \text{ nm}$, in the range of 2θ angles 20–90°. The step size during the scan was 0.1°. IR spectra in the 400–4000 cm^{-1} were obtained with a Fourier spectrometer Bruker Optics-Vertex 70V Billerica, MA, USA. Measurements were made using the powder technique. Absorption of the spectrum was recorded at 128 scans with a resolution of 4 cm^{-1} . To characterize critical temperatures of transformations taking place in the obtained samples (T_g —transformation temperature (glass transition)), T_c —crystallization temperature, T_m —melting point), thermal analyses (Dilatometric, DSC) were performed. Dilatometric tests were realized using a Sadamel DA-3 Switzerland dilatometer, while DSC tests were carried out using a NETZSCH DSC-TG STA 449 F3 Jupiter, Selb, Germany; thermoanalyzer. The glass samples were heated at the rate of 10 °C/min, in the temperature range of 25 ÷ 1200 °C, in an air atmosphere. The analysis was performed in Al_2O_3 crucibles. Moreover, thermal tests allowed to determine stability parameters of the tested glasses according to Hruby (K_H), Angell (K_A) and Saad-Poulain (K_{SP}) equations (Equations (1)–(3)) [39–41]. The process of directed crystallization of the melted amphibolite glasses was carried out at the following parameters: time 5 and 10 h, temperature 800 °C, 900 °C and 1000 °C. In addition, to determine the changes taking place as a consequence of the directed crystallization process on the structure and properties of amphibolite glasses, XRD and SEM-EDS examinations using a JOEL JSM-6610LV, Peabody, MA, USA; scanning microscope were performed. Microhardness tests were performed both for the as-received glasses and glasses after heat treatment. The Vickers microhardness values were measured using a SHIMADZU, Kyoto, Japan; microhardness tester under a load of 50 g. The dwell time of 10 s was constant for all the samples. Microhardness values were calculated using the following equation: $\text{HV} = A (p/d^2) \text{ kg/mm}^2$, where A is a constant equal to 1854.5, p is the applied load (g), and d is the average diagonal length (μm); and converted from kg/mm^2 to MPa. Viscosity was determined for all tested glasses using the one-point method, where the base for viscosity curve determination is the T_g temperature received from the DSC analysis. The viscosity of the tested glasses was then determined using the relationship initially presented in Formula (4) [42].

3. Results and Discussion

3.1. Study of Amphibolite Glasses after the Melting Process

In the first stage of the research, after the melting process of the prepared glass sets, XRD phase analysis was performed, and the chemical composition was determined using the XRF method. The analyses performed are presented in Figure 2 and Table 2. The diffractograms showed only an increased background in the range of 30–50°, characteristic of amorphous materials, which confirms that an amorphous material-glass—was obtained in the melting stage [43].

The chemical composition analysis of the obtained glasses confirmed that they are multicomponent aluminosilicate glasses of the SiO_2 - Al_2O_3 - MgO - CaO system. As can be seen from the literature data, research on this type of glasses focused, among others, on their application to the production of glass-crystalline materials, very often obtained based on waste materials from the construction industry [44,45]. The results of structural studies with

FTIR spectroscopy of the produced amphibolite glasses with different dolomite contents are presented in Figure 3.

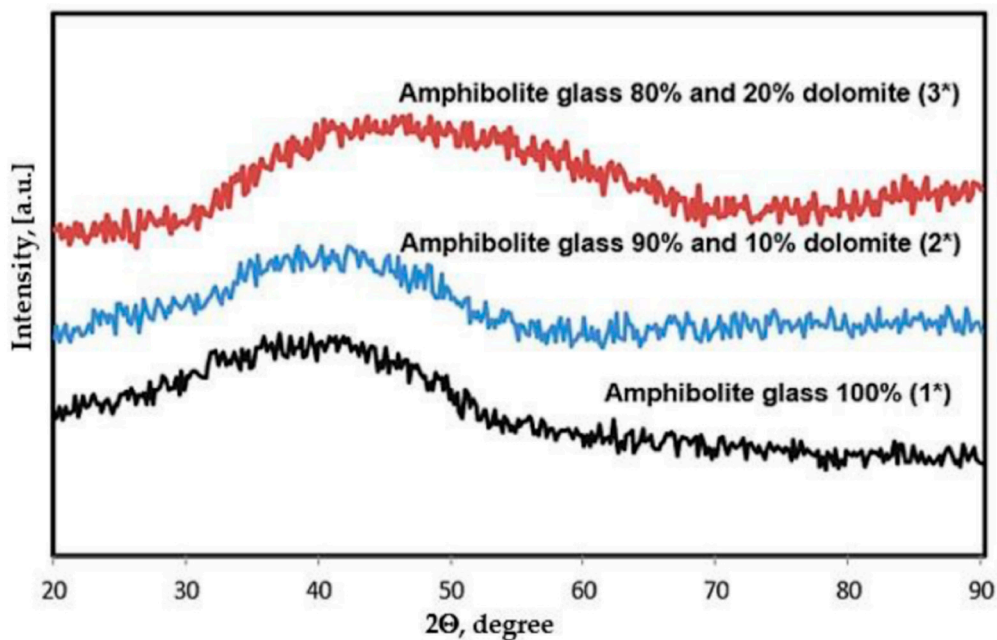


Figure 2. X-ray diffractograms of amphibolite glasses after the melting process.

Table 2. Chemical composition of amphibolite glasses after the melting process [wt.%].

Glass	Component, [wt.%]											
	SiO ₂	Al ₂ O ₃	CaO	MgO	Fe ₂ O ₃	K ₂ O	Na ₂ O	TiO ₂	P ₂ O ₅	MnO	ZrO ₂	SO ₃
Set 1* Amphibolite Glass	54.6	14.1	6.08	4.78	10.3	0.22	5.41	1.08	0.10	0.25	0.10	0.10
Set 2* Amphibolite Glass 90 wt.%/Dolomite 10 wt.%	49.47	12.83	11.41	8.00	9.35	0.22	4.91	0.98	0.09	0.24	0.11	0.10
Set 3* Amphibolite Glass 80 wt.%/Dolomite 20 wt.%	44.33	11.55	16.73	11.21	8.41	0.21	4.40	0.87	0.09	0.24	0.12	0.09

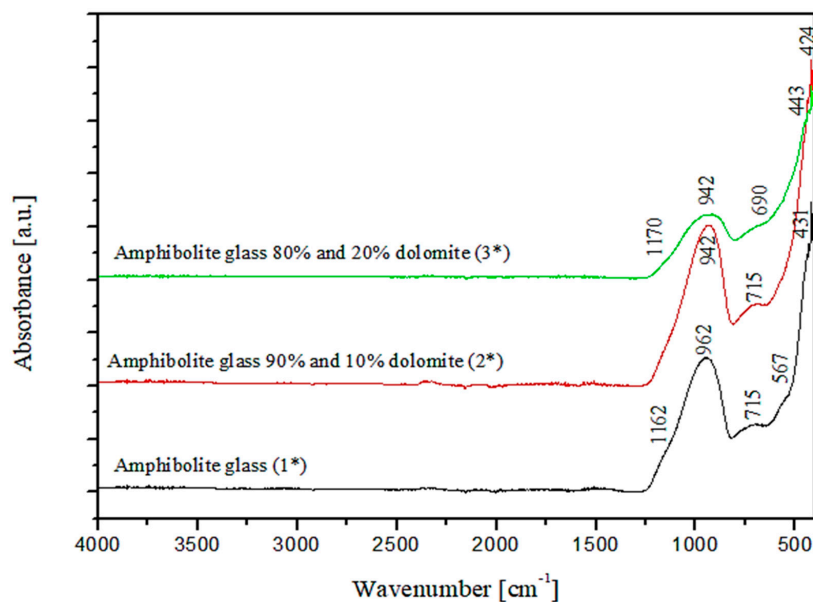


Figure 3. FTIR spectra of amphibolite glasses after the melting process.

Three main absorption bands are visible in the FTIR spectra of the studied amphibolite glasses. Peaks are located at approx. 962 (942), 715 (690) and 431 (443/424) cm^{-1} . The most intense bands, located in the range 1400–800 cm^{-1} are attributed to asymmetric stretching vibrations of two bond types: Si-O-(Si), and (Al) [46]. Much less intense complex bands in the range of 800–650 cm^{-1} correspond to symmetric bending vibrations of Si-O-Si and Si-O-Al [47]. The band located in the range of 550–400 cm^{-1} can be related to bending vibrations originating from O-Si-O and O-Al-O [48,49]. The first group is the most sensitive to changes in a lattice structure and usually represents a superposition of several bands located close to each other [50]. Based on the obtained spectra, it was observed that adding dolomite and introducing CaO and MgO oxides at the expense of SiO_2 , causes the breaking of some of the Si-O-Si and Si-O-Al bonds. The network depolymerizes under the influence of modifiers, which is particularly evident in the case of glass modified with 20 wt.% dolomite addition, where a significant decrease in half-width of bands in the wavenumber range 1400–800 cm^{-1} is visible and a shift of all bands towards lower wavenumber values. In the next step of the research, transformation temperatures (T_g , T_c , T_m) of the glasses were determined by DSC thermal analysis as shown in Figures 4–6. In the case of the 100% amphibolite (Set 1*) sample, the transformation temperature could not be accurately determined from the DSC curve, so additional dilatometric tests were carried out finally to determine T_g (Figure 7).

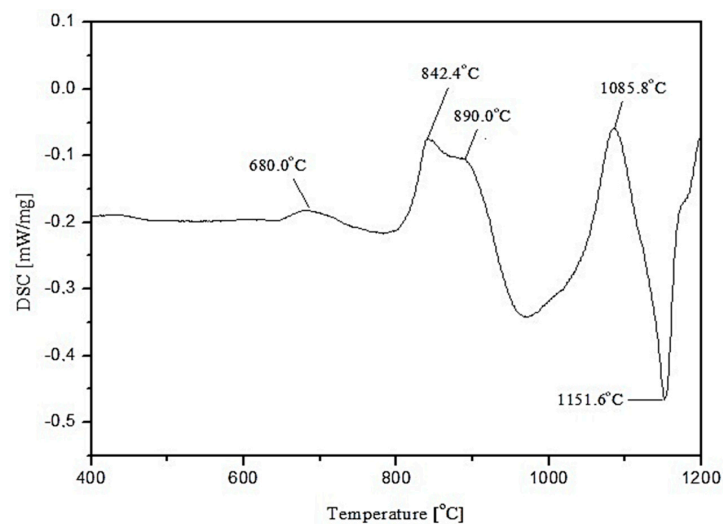


Figure 4. DSC curve of 100 wt.% amphibolite glass (Set 1*).

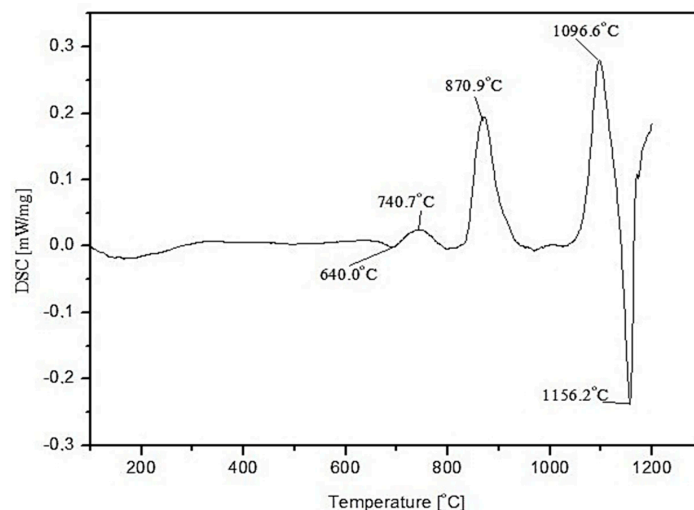


Figure 5. DSC curve of amphibolite glass with 10 wt.% dolomite addition (Set 2*).

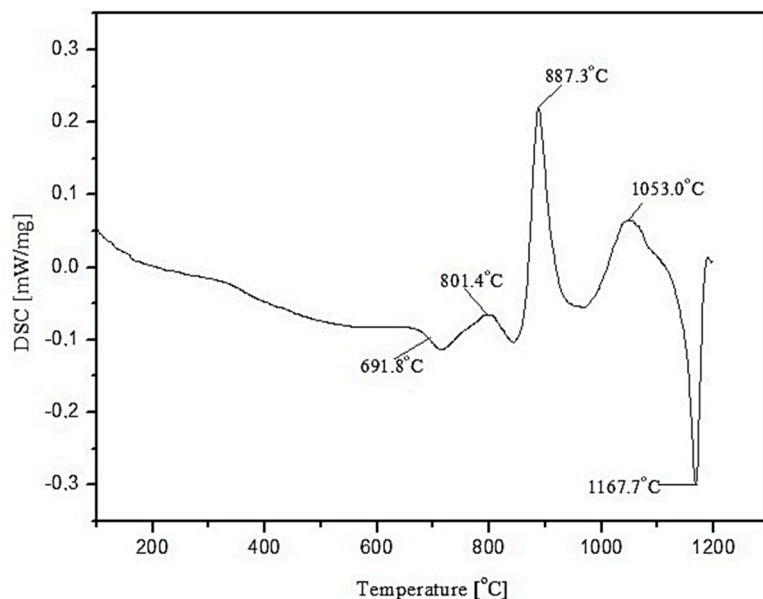


Figure 6. DSC curve of amphibolite glass with 20 wt.% dolomite addition (Set 3*).

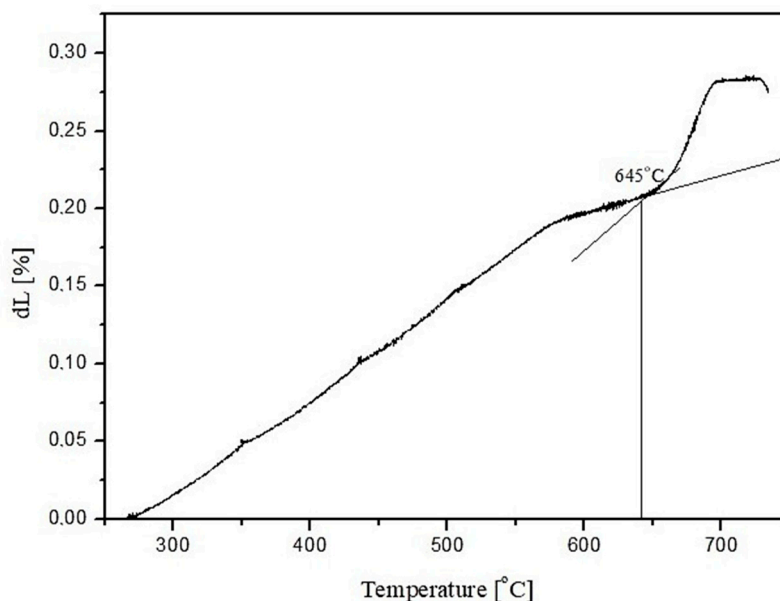


Figure 7. Dilatometric curve of 100 wt.% amphibolite glass (Set 1*).

The thermal analysis results were used to determine the basic parameters of the thermal stability of the glasses according to Hruby (K_H), Angell (K_A) and Saad-Poulain (K_{SP}) using the following equations [39,40]:

$$K_H = \frac{T_c - T_g}{T_m - T_c} \tag{1}$$

$$K_A = T_c - T_g \tag{2}$$

$$K_{SP} = \frac{(T_c - T_g)(T_{cmax} - T_c)}{T_g} \tag{3}$$

where: T_g —glass transition temperature, T_c —crystallization start temperature, T_{cmax} —crystallization maximum temperature, T_m —melting point.

The Angell parameter (K_A) is a simple relationship; it only considers the difference between crystallization and glass transition temperatures. On the other hand, according to Hruby and Saad-Poulaine, the relationships are more complex. They take into account other correlations affecting the propensity to vitrification and consider the three most essential transformation temperatures during glass heating (T_g , T_c , T_m). Table 3 summarizes the DSC results together with the glass stability parameters.

Table 3. Characteristic temperatures of studied amphibolite glasses determined by DSC thermal analysis.

Glass	T_g [°C]	T_{c1} [°C]	T_{c1max} [°C]	T_{c2max} [°C]	T_{c3max} [°C]	T_m [°C]	K_A	K_H	K_{SP}
Set 1* 100 wt.% Amphibolite	645	665	681	842	1086	1151	20	0.04	0.50
Set 2* 90 wt.% Amphibolite/10 wt.% Dolomite	640	675	741	871	1097	1156	35	0.07	3.61
Set 3* 80 wt.% Amphibolite/20 wt.% Dolomite	692	710	801	887	1050	1168	18	0.04	2.37

The thermal analysis results showed that modifying the amphibolite glasses with dolomite changes their characteristic temperatures and thus affects thermal stability. DSC curves showed that the glass transition temperature (T_g) of the obtained amphibolite glasses is between 640–690 °C. Exothermic processes related to glass crystallization were visible at higher temperatures, which depends mainly on the chemical composition. Additionally, the multiphase crystallization process was recorded for all the amphibolite glasses. The exothermic crystallization effect was the weakest and broad for the unmodified amphibolite glass (Set 1*), thus, the most intensive crystallization effect was observed for glass modified with 20 wt.% dolomite addition (Set 3*). For the studied glasses, it is also characteristic that an endothermic effect is visible after the exothermic effect related to the complete or partial melting of the crystalline phases. In general, the applied modification of glasses with dolomite had a positive effect on the material's thermal stability. The addition of dolomite in the amount of 10 wt.% (Set 2*) caused an increase in the values of K_A and K_H , K_{SP} parameters in comparison to pure amphibolite glass (Set 1*). The higher values of these parameters indicate a decrease in the glass's ability to crystallize, which is beneficial, e.g., in mineral fibre production. On the other hand, an increase in the proportion of dolomite to 20 wt.% increases the glass transition temperature from 640 °C (Set 1*) to 692 °C (Set 3*), with a simultaneous decrease in glass stability. It is known that MgO in the glass structure can take both the coordination numbers 6 and 4 [51,52]. This means that it can act as a modifying ion (LK 6) similarly to CaO, or build into the network as a bond-forming ion (LK4). In the case of glasses containing in their chemical composition a high proportion of metal ions that can occur in different coordination numbers, any increase in the amount of free oxygen in the glass mass favours the adoption of lower coordination by these ions. The increase of metal ions in coordination number 4 results in the incorporation of these ions into the glass bond, thus strengthening it, which contributes to an increase in the stability of glass with 20% dolomite addition [53]. According to literature data, the higher K_H value for glass, the higher its resistance to crystallization during heating and ability to vitrify during cooling [54,55]. A lowering of the K_{SP} , K_A , and K_H values implies a higher ability to crystallize, which is particularly important during the lifetime of the glasses, depending on their intended use. However, in the case of mineral fibres, this can contribute to crushing and loss of the required strength properties [56].

3.2. Study of Amphibolite Glasses after the Crystallization Process

The DSC results shown in Table 3 were used to determine the parameters of the directed crystallization process, which were ultimately carried out for temperatures of

800 °C, 900 °C and 1000 °C and times 5 and 10 h. The structural investigation results using XRD and FTIR spectroscopic analysis for the crystallized glasses are shown in Figures 8–10.

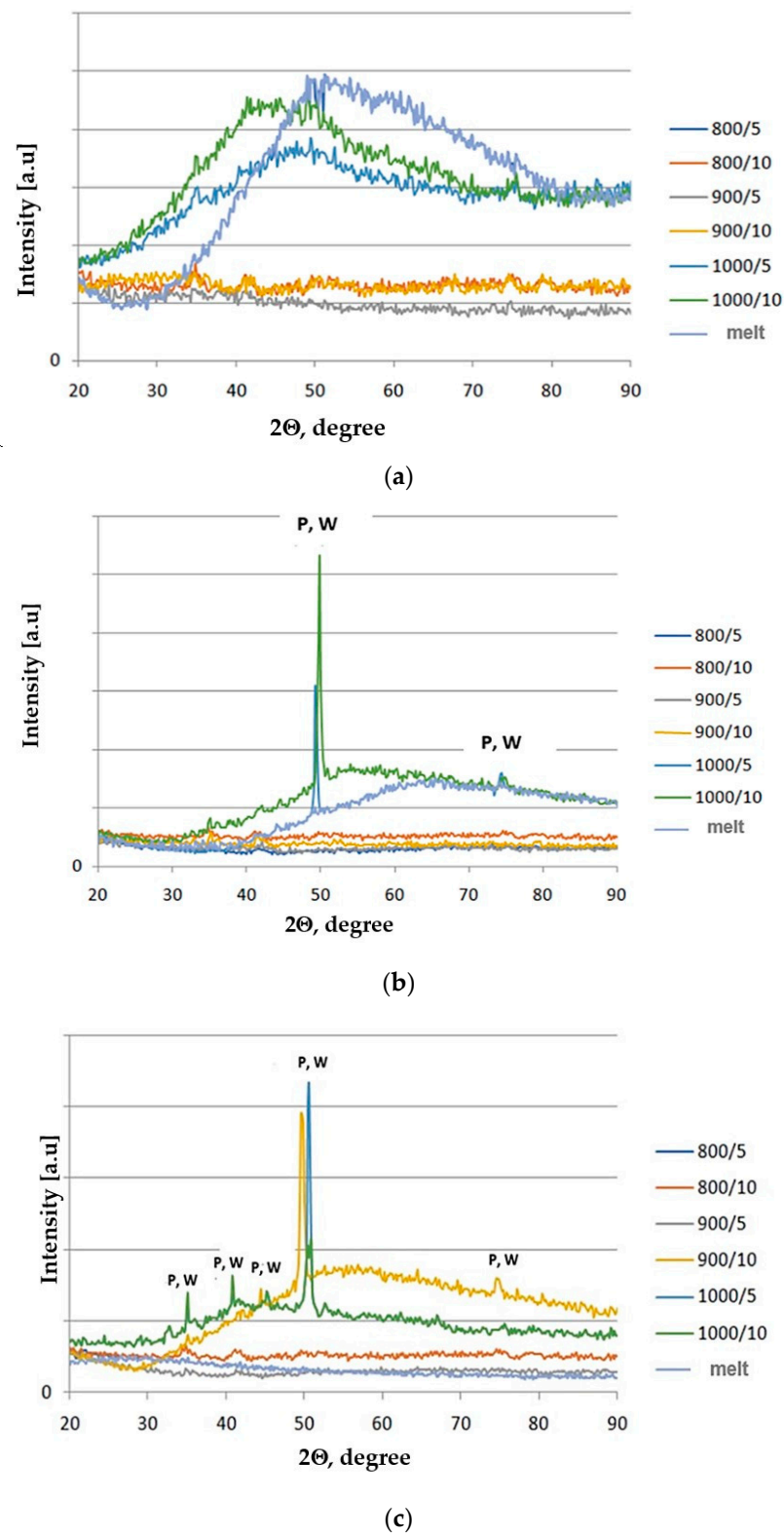


Figure 8. X-ray diffractograms of amphibolite glasses after after crystallization process: (a) 100 wt.% amphibolite (Set 1*), (b) 90 wt.% amphibolite + 10 wt.% dolomite (Set 2*), (c) 80 wt.% amphibolite + 20 wt.% dolomite (Set 3*); P—Pyroxene, W—Wollastonite.

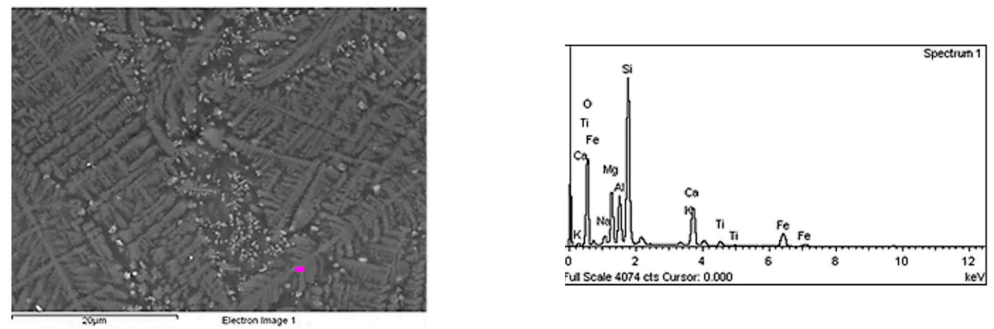
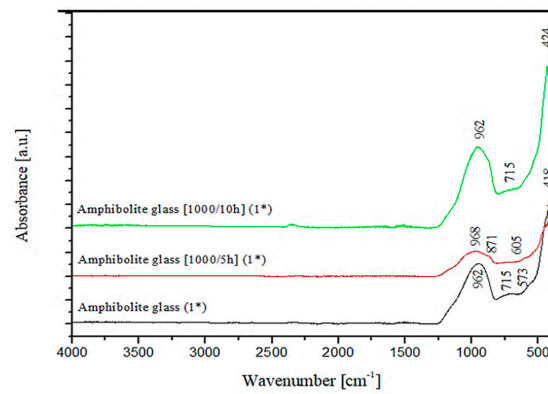
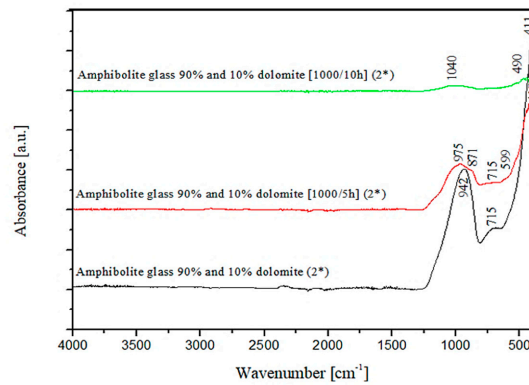


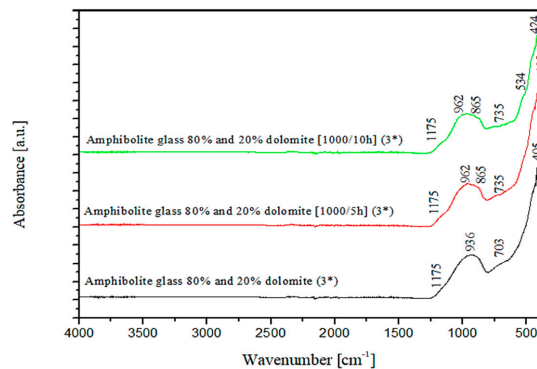
Figure 9. SEM-EDS image and analysis of amphibolite glass modified with 20 wt.% dolomite addition (Set 3*) after crystallization at 1000 °C for 10 h.



(a)



(b)



(c)

Figure 10. FTIR of amphibolite glasses selected before and after crystallization process: (a) 100 wt.% amphibolite (1*), (b) 90 wt.% amphibolite + 10 wt.% dolomite (2*), (c) 80 wt.% amphibolite + 20 wt.% dolomite (3*).

The XRD results confirmed the amorphous character only for a glass containing 100 wt.% amphibolite both after the melting and crystallization processes. This is evidenced by the visible raised, extended background at 34–50° (Figure 8a–c). In the glasses modified with dolomite after the crystallization process, apart from the increased background, peaks characteristic of amorphous materials were observed, confirming the presence of crystalline phases. Based on the analysis, it was found that the phases are represented mainly by pyroxenes (diopside (Ca(Mg,Al)(Si,Al)₂O₆; JCPDS no. 41-1370) and wollastonite (CaSiO₃, JCPDS no. 043-1460). The main crystalline phase is pyroxenes (augite, diopside). The addition of dolomite introduced additional Ca⁺ and Mg⁺ ions into the glasses, contributing to the crystallization of pyroxene phases. Pyroxenes are minerals with various chemical compositions. A wide variety of ionic and isomorphous substitutions of multiple elements occurs among the group of pyroxenes. Some of the Al³⁺ ions from the base glass can enter the pyroxene structures, replacing the Mg²⁺ and Si⁴⁺ [57]. The Ca²⁺ ion is one of the major ions, and its effective radius is close to Pb²⁺ and Ba²⁺, which exhibits minimal mobility in the glass lattice. At the same time, Mg²⁺ has a smaller size and greater mobility. Therefore, the rate of diffusion of Ca²⁺ ions mainly determines the formation of diopside [58]. In the case of the glasses modified with the 10 wt.% addition of dolomite, peaks from the crystalline phases appear only at 1000 °C for the glasses heated for 5 and 10 h. For the glasses with the 20 wt.% addition of dolomite, peaks appear at 900 °C after 10 h of heating, indicating crystalline phase formation. These results confirm that the addition of dolomite increases the ability of amphibolite glasses to crystallize. However, a higher dolomite content reduces the thermal stability of the glasses. Figure 9 shows the microstructure of the amphibolite glass obtained from Set 3*, after the crystallization process (1000 °C/10 h). The obtained SEM-EDS results confirmed the XRD studies that pyroxenes are the main crystallizing phase in the examined multicomponent amphibolite glasses.

After the directed crystallization process, the amphibolite glasses' spectroscopic studies with FTIR showed slight changes (Figure 10). In addition to the three main bands discussed in the spectra of the base glass (Figure 3), broadening of the bands in the range of 1400–850 cm⁻¹ and a division into two bands at values of approx. 962 and approx. 865 cm⁻¹ was observed. This proves the formation of crystalline phases in the crystallization process of the glasses—mainly pyroxenes—in the diopside band at 865 cm⁻¹ [59,60]. The bands in the range 800–650 cm⁻¹ for glass after directed crystallization (1000 °C/10 h) show spectra with a hardly visible significant half-width. These changes confirm the depolymerization of the glass lattice, a loss of Si-O-Si, Si-O-Al [61].

The results of the DSC thermal analysis were also used to determine the viscosity of the multicomponent amphibolite glasses (Table 4), a parameter that is very important from the point of view of glass fibre production. The one-point method was used to determine the parameter, where the transformation temperature (T_g) is used to determine the viscosity of the glass, according to the relation [42]:

$$\log \eta = 13.4 - C_1 + \frac{C_1 C_2}{T - T_g + C_2} \quad (4)$$

where: T—test temperature [°C], T_g—transformation temperature (determined for the tested glasses) C₁, C₂—constant.

The dependence of the glass viscosity on the chemical composition allows two areas of viscosity to be distinguished: low-temperature $\eta > 10^6$ dPas, affecting the crystallization of the glasses, and high-temperature, within the limits of $\eta < 10^6$ dPas, important from the point of view of the melting and fibre formation process. Dolomite addition to the amphibolite glass in the amount of 10 wt.% slightly reduces the viscosity of the glass. On the other hand, increasing the amount of dolomite to 20 wt.% causes a slight increase in viscosity in the entire temperature range. In the investigated glasses, the sum of the oxides of alkali metals and alkaline earth metals is greater than the alumina content. Ratio $[R_2O+RO]/[Al_2O_3] > 1$ (Table 2). It is known that Al₂O₃ can be a glass-forming component [62], and when Al³⁺ ions enter the [AlO₄] structure, there should be enough

alkali metal and alkaline earth metal cations to maintain the electric charge balance. Based on literature data, it is known that Ca^{2+} ions take precedence over Mg^{2+} ions in charge of the compensation of Al^{3+} ions and lead to the formation of more stable $\text{Ca}[\text{AlO}_4]^{5-}$ tetrahedral structures, which in turn results in increased viscosity $> 10^6$ dPas, important from the point of view of the melting and fibre formation process [63,64].

Table 4. Viscosity coefficients of glasses determined by the one-point method.

Glass	Temperature, °C											
	660	700	740	860	900	940	980	1020	1060	1100	1140	1180
	$\log \eta$, dPas											
Amphibolite glass $T_g = 640$ °C	13.6	11.4	9.8	6.5	5.8	5.2	4.6	4.2	3.8	3.4	3.2	2.8
Amphibolite glass 90 wt.% /10 wt.% Dolomite, $T_g = 645$ °C	13.0	11.0	9.4	6.3	5.6	5.0	4.5	4.1	3.7	3.3	3.0	2.7
Amphibolite glass 80 wt.% /20 wt.% Dolomite, $T_g = 692$ °C	14.3	12.0	10.2	6.8	6.0	5.3	4.8	4.3	3.9	3.5	3.3	2.9

The results of microhardness tests of amphibolite glasses by the Vickers method (Table 5) showed that the microhardness of amphibolite glasses increases with dolomite content. Moreover raising the MgO and CaO content at the expense of SiO_2 also improves the microhardness of the glasses [65,66] same as the increasing proportion of crystalline phases in the glass matrix for crystalline glasses [67]. This is particularly evident in the case of glasses after the crystallization process modified with 20 wt.% dolomite addition (Set 3*).

Table 5. Vickers microhardness results for amphibolite glasses after melting and the crystallization process.

Melt/Crystallization Parameters [°C]/Time h	Type of Glass		
	Set 1 Amphibolite Glass 100 wt.%	Set 2 Amphibolite Glass 90 wt.% Dolomite 10 wt.%	Set 3 Amphibolite Glass 80 wt.% Dolomite 20 wt.%
	HV 0.05	HV 0.05	HV 0.05
Melt (glass)	690	751	769
800/5	693	756	773
800/10	695	712	757
900/5	711	759	805
900/10	773	840	871
1000/5	736	813	835
1000/10	745	807	855

4. Conclusions

Based on the results, it was found that the modification of amphibolite glasses with dolomite in various proportions affects their structure and properties. The structure of the glasses studied changed depending on the amount of dolomite in the glass and the conditions of the crystallization process carried out. The glass stability coefficients determined from the results of DSC thermal analysis showed that at a dolomite content of 10 wt.% the glass stability is higher than that of pure amphibolite glass (Set 1*). In addition, dolomite reduces viscosity, which is very beneficial in the context of mineral fibre production. The crystallization process carried out showed that the crystalline phases in the studied glasses are mainly represented by pyroxenes-diopside and wollastonite. In the case of the addition of 10 wt.% of dolomite, the crystalline phases appear only at a temperature of 1000 °C, whereas when the dolomite content is 20 wt.%, the glass crystallizes already at

a temperature of 900 °C. Moreover, when analyzing microhardness results, it was found that the addition of dolomite and optimization of the crystallization process increases the strength of amphibolite glasses, which is very important for the production of mineral fibres for many industrial sectors. The authors conduct further research on amphibolite glasses focusing on applications in the construction industry, including insulation materials, as well as reinforcement of composites, and building materials for structural applications.

Author Contributions: Conceptualization, A.N. and M.L.; Methodology, A.N. and M.L.; Data analysis and validation, A.N., M.L., M.S. and J.I.; Performing research and investigation, M.L., A.N., R.C., M.S., K.K. and J.I.; Writing—original draft preparation, M.L., A.N. and J.J.J.; Supervision, M.L. and J.I.; Funding acquisition, M.L. and J.J.J. All authors have read and agreed to the published version of the manuscript.

Funding: This research received no external funding.

Institutional Review Board Statement: Not applicable.

Informed Consent Statement: Not applicable.

Data Availability Statement: The data presented in this study are available on request from the corresponding author. The data are not publicly available due to the possibility of use in further research.

Conflicts of Interest: The authors declare no conflict of interest.

References

1. Khater, G. Glass-ceramics in the CaO–MgO–Al₂O₃–SiO₂ system based on industrial waste materials. *J. Non-Cryst. Solids* **2010**, *356*, 3066–3070. [[CrossRef](#)]
2. Barbieri, L.; Corradi, A.; Lancellotti, I.; De Oliveira, A.P.N.; Alarcon, O.E. Nucleation and crystal growth of a MgO–CaO–Al₂O₃–SiO₂ Glass with Added Steel Fly Ash. *J. Am. Ceram. Soc.* **2004**, *85*, 670–674. [[CrossRef](#)]
3. Rincón, J.M. Vitreous and ceramic processing for the recycling of industrial wastes. *Key Eng. Mater.* **2016**, *663*, 11–22. [[CrossRef](#)]
4. Korwin-Edson, M.L.; Hofmann, D.A.; McGinnis, P.B. Strength of high performance glass reinforcement fiber. *Int. J. Appl. Glas. Sci.* **2012**, *3*, 107–121. [[CrossRef](#)]
5. Zhang, Y.F.; Vulfson, Y.; Zheng, Q.J.; Luo, J.W.; Kim, S.H.; Yue, Y.Z. Impact of fiberizing method on physical properties of glass wool fibers. *J. Non-Cryst. Solids* **2017**, *476*, 122–127. [[CrossRef](#)]
6. Li, H.; Richards, C.; Watson, J. High-performance glass fiber development for composite applications. *Int. J. Appl. Glas. Sci.* **2013**, *5*, 65–81. [[CrossRef](#)]
7. Monaldo, E.; Nerilli, F.; Vairo, G. Basalt-based fiber-reinforced materials and structural applications in civil engineering. *Compos. Struct.* **2019**, *214*, 246–263. [[CrossRef](#)]
8. Ivanič, A.; Kravanja, G.; Kidess, W.; Rudolf, R.; Lubej, S. The Influences of Moisture on the Mechanical, Morphological and Thermogravimetric Properties of Mineral Wool Made from Basalt Glass Fibers. *Materials* **2020**, *13*, 2392. [[CrossRef](#)]
9. Yliniemi, J.; Kinnunen, P.; Karinkanta, P.; Illikainen, M. Utilization of Mineral Wools as Alkali-Activated Material Precursor. *Materials* **2016**, *9*, 312. [[CrossRef](#)]
10. Papadopoulos, A. State of the art in thermal insulation materials and aims for future developments. *Energy Build.* **2005**, *37*, 77–86. [[CrossRef](#)]
11. Wei, B.; Cao, H.; Song, S. Tensile behavior contrast of basalt and glass fibers after chemical treatment. *Mater. Des.* **2010**, *31*, 4244–4250. [[CrossRef](#)]
12. Gunschera, J.; Sibel, M.; Salthammer, T.; Andersen, J.R. Impact of building materials on indoor formaldehyde levels: Effect of ceiling tiles, mineral fiber insulation and gypsum board. *Build. Environ.* **2013**, *64*, 138–145. [[CrossRef](#)]
13. Karamanos, A.; Hadiarakou, S.; Papadopoulos, A.M. The impact of temperature and moisture on the thermal performance of stone wool. *Energy Build.* **2008**, *40*, 1402–1411. [[CrossRef](#)]
14. Drozdyuk, T.; Aizenshtadt, A.; Tutygin, A.; Frolova, M. *Basalt Fiber Insulating Material with a Mineral Binding Agent for Industrial Use*; MEACS2015 IOP Publishing IOP Conference Series Materials: Materials Science and Engineering; IOP: Bristol, UK, 2016; Volume 124, p. 012123. [[CrossRef](#)]
15. Toman, J.; Vimmrová, A.; Černý, R. Long-term on-site assessment of hygrothermal performance of interior thermal insulation system without water vapour barrier. *Energy Build.* **2009**, *41*, 51–55. [[CrossRef](#)]
16. Vrána, T.; Gudmundsson, K. Comparison of fibrous insulations—Cellulose and stone wool in terms of moisture properties resulting from condensation and ice formation. *Constr. Build. Mater.* **2010**, *24*, 1151–1157. [[CrossRef](#)]
17. Jerman, M.; Černý, R. Effect of moisture content on heat and moisture transport and storage properties of thermal insulation materials. *Energy Build.* **2012**, *53*, 39–46. [[CrossRef](#)]

18. Vrána, T.; Björk, F. Frost formation and condensation in stone-wool insulations. *Constr. Build. Mater.* **2009**, *23*, 1775–1787. [[CrossRef](#)]
19. Fiore, V.; Scalici, T.; Di Bella, G.; Valenza, A. A review on basalt fibre and its composites. *Compos. Part B Eng.* **2015**, *74*, 74–94. [[CrossRef](#)]
20. Dhand, V.; Mittal, G.; Rhee, K.Y.; Park, S.-J.; Hui, D. A short review on basalt fiber reinforced polymer composites. *Compos. Part B Eng.* **2015**, *73*, 166–180. [[CrossRef](#)]
21. Deák, T.; Czigány, T. Chemical composition and mechanical properties of basalt and glass fibers: A comparison. *Text. Res. J.* **2009**, *79*, 645–651. [[CrossRef](#)]
22. Gutnikov, S.I.; Malakho, A.P.; Lazoryak, B.I.; Loginov, V.S. Influence of alumina on the properties of continuous basalt fibers. *Russ. J. Inorg. Chem.* **2009**, *54*, 191–196. [[CrossRef](#)]
23. Manylov, M.S.; Gutnikov, S.I.; Lipatov, Y.V.; Malakho, A.P.; Lazorya, B.I. Effect of deferrization on continuous basalt fiber properties. *Mendeleev Commun.* **2015**, *25*, 386–388. [[CrossRef](#)]
24. Manylov, M.S.; Gutnikov, S.; Pokholok, K.V.; Lazoryak, B.I.; Lipatov, Y.V. Crystallization mechanism of basalt glass fibers in air. *Mendeleev Commun.* **2013**, *23*, 361–363. [[CrossRef](#)]
25. Tatarintseva, O.; Khodakova, N.; Uglova, T. Dependence of the viscosity of basalt melts on the chemical composition of the initial mineral material. *Glass Ceram.* **2012**, *68*, 323–326. [[CrossRef](#)]
26. Bauera, F.; Kempfa, M.; Weiland, F.; Middendorf, P. Structure-property relationships of basalt fibers for high performance applications. *Compos. Part B Eng.* **2018**, *145*, 121–128. [[CrossRef](#)]
27. Kochergin, A.V.; Granovskaya, N.V.; Kochergin, D.V.; Savchenko, V.A.; Galimov, N.R. Ways to supply gabbro-basalt raw materials to mineral fiber producers. *Glas. Ceram.* **2013**, *69*, 405–408. [[CrossRef](#)]
28. Širok, B.; Bullen, F.P.; Blagojević, B. *Mineral Wool: Production and Properties*; Woodhead Publishing: Cambridge, UK; p. 192. Available online: <http://public.ebookcentral.proquest.com/choice/publicfullrecord.aspx?p=1639563> (accessed on 12 May 2022).
29. Lubas, M.; Wyszomirski, P. Niekonwencjonalne wykorzystanie amfibolitów dolnośląskich/Unconventional use of Lower Silesian amphibolites. *Mater. Ceram. Ceram. Mater.* **2009**, *61*, 31–34.
30. Maliszewski, M.; Pomorski, A.; Cichoń, T. Możliwości wykorzystania trudno zbywalnych frakcji amfibolitu ze złoża pagórki wschodnie/Possibilities of utilization of difficult-to-market amphibolite fractions from the pagórki wschodnie deposit. *Górnictwo Odkryw.* **2017**, *5*, 4–10.
31. Bodnárová, L.; Ťažký, M.; Ťažká, L.; Hela, R.; Pikna, O.; Sitek, L. Abrasive Wear Resistance of Concrete in Connection with the Use of Crushed and Mined Aggregate, Active and Non-Active Mineral Additives, and the Use of Fibers in Concrete. *Sustainability* **2020**, *12*, 9920. [[CrossRef](#)]
32. Operta, M. Non-metallic mineral resources in the Vareš region. *Acta Geogr. Bosniae Herzeg.* **2015**, *3*, 35–42.
33. Lampropoulou, P.; Papoulis, D.; Metaxa, E.; Tsikouras, B.; Hatzipanagioutou, K.; Tzeveleku, T.H.; Karageorgis, A. Assessment of the quality of metamorphic and igneous rocks from terpni (serres, north greece) for their use as raw materials in the production of stonewool. *Bull. Geol. Soc. Greece* **2016**, *50*, 1913–1922. [[CrossRef](#)]
34. Kibol, V.; Kibol, R. Method for Producing Fibers from Rocks and a Plant for Carrying Out Said Method. U.S. Patent 12/866,475, 16 December 2010.
35. Schinking, T.; Mayer, A. Raw Material for Producing Basalt Fibers. U.S. Patent 9,073,780, 12 December 2013.
36. Bąk, B.; Radwanek-Bąk, B.; Wyszomirski, P. Aktualny przegląd krajowych złóż dolomitów w aspekcie wykorzystania w przemyśle materiałów ogniotrwałych/Current overview of domestic dolomite deposits in terms of use in refractory industry. *Gospod. Surowcami Miner.* **2011**, *27*, 21–45.
37. Yue, Y.; Zheng, G. Fiber spinnability of glass melts. *Int. J. Appl. Glas. Sci.* **2017**, *8*, 37–47. [[CrossRef](#)]
38. Lund, M.D.; Yue, Y. Impact of drawing stress on the tensile strength of oxide glass fibers. *J. Am. Ceram. Soc.* **2010**, *93*, 3236–3243. [[CrossRef](#)]
39. Nascimento, M.L.F.; Souza, L.A.; Ferreira, E.B.; Zanutto, E.D. Can glass stability parameters infer glass forming ability? *J. Non-Cryst. Solids* **2005**, *351*, 3296–3308. [[CrossRef](#)]
40. Hrubý, A. Evaluation of glass-forming tendency by means of DTA. *Czechoslov. J. Phys.* **1972**, *22*, 1187–1193. [[CrossRef](#)]
41. Kozmidispetrovic, A.; Šesták, J. Forty years of the Hrubý glass-forming coefficient via DTA when comparing other criteria in relation to the glass stability and vitrification ability. *J. Therm. Anal.* **2012**, *110*, 997–1004. [[CrossRef](#)]
42. Fotheringham, U. *Viscosity of Glass and Glass-Forming Melts*; Springer Handbook of Glass: Springer Handbooks; Springer: Cham, Switzerland; pp. 79–112. [[CrossRef](#)]
43. Kang, J.; Cheng, J.; Lou, X.; Tian, P.; Liu, K. Fabrication and Characterization of Diopside-based Glass-Ceramics from Granite Wastes. *Trans. Indian Ceram. Soc.* **2015**, *74*, 218–224. [[CrossRef](#)]
44. Effendy, E.; Abdul Wahab, Z.; Mohamed Kamari, H.; Matori, K.A.S.; Ab Aziz, H.J.; Zaid, M.H.M. Structural and optical properties of Er³⁺-doped willemite glass-ceramics from waste materials. *Optik* **2016**, *127*, 11698–11705. [[CrossRef](#)]
45. Wang, S.; Zhang, C.; Chen, J. Utilization of coal fly ash for the production of glass-ceramics with unique performances: A brief review. *J. Mater. Sci. Technol.* **2014**, *30*, 1208–1212. [[CrossRef](#)]
46. Sitarz, M. The structure of simple silicate glasses in the light of Middle Infrared spectroscopy studies. *J. Non-Cryst. Solids* **2011**, *357*, 1603–1608. [[CrossRef](#)]

47. Kucharczyk, S.; Sitarz, M.; Zajac, M.; Deja, J. The effect of CaO/SiO₂ molar ratio of CaO-Al₂O₃-SiO₂ glasses on their structure and reactivity in alkali activated system. *Spectrochim. Acta Part A Mol. Biomol. Spectrosc.* **2018**, *194*, 163–171. [[CrossRef](#)]
48. Partyka, J.; Sitarz, M.; Leśniak, M.; Gasek, K.; Jeleń, P. The effect of SiO₂/Al₂O₃ ratio on the structure and microstructure of the glazes from SiO₂-Al₂O₃-CaO-MgO-Na₂O-K₂O system. *Spectrochim. Acta Part A Mol. Biomol. Spectrosc.* **2015**, *134*, 621–630. [[CrossRef](#)] [[PubMed](#)]
49. Yang, Z.; Lin, Q.; Lu, S.; He, Y.; Liao, G.; Ke, Y. Effect of CaO/SiO₂ ratio on the preparation and crystallization of glass-ceramics from copper slag. *Ceram. Int.* **2014**, *40*, 7297–7305. [[CrossRef](#)]
50. Stoch, L.; Wacławska, I.; Środa, M. Thermal study of the influence of chemical bond ionicity on the glass transformation in (Na₂O, CaO, MgO)-Al₂O₃-SiO₂ glasses. *J. Therm. Anal.* **2004**, *77*, 57–63. [[CrossRef](#)]
51. Fang, Y.; Zheng, Z.; Yanling, Z.; Tuo, W. Effect of Al₂O₃ content on the viscosity and structure of CaO-SiO₂-Cr₂O₃-Al₂O₃ slags. *Int. J. Miner. Metall. Mater.* **2021**, *29*, 1522–1531. [[CrossRef](#)]
52. Zawada, A.; Lubas, M.; Przerada, I.; Sitarz, M.; Adamczyk-Habrajska, M. The effect of the reducing melting atmosphere on coordination moieties in aluminosilicate glasses. *J. Mol. Struct.* **2020**, *1218*, 128474. [[CrossRef](#)]
53. Lü, J.F.; Jin, Z.N.; Yang, H.Y.; Tong, L.L.; Chen, G.B.; Xiao, F.X. Effect of the CaO/SiO₂ mass ratio and FeO content on the viscosity of CaO-SiO₂-FeO-12 wt% ZnO-3 wt% Al₂O₃ slags. *Int. J. Miner. Metall. Mater.* **2017**, *24*, 756–767. [[CrossRef](#)]
54. Joseph, K.; Jolley, K.; Smith, R. Iron phosphate glasses: Structure determination and displacement energy thresholds, using a fixed charge potential model. *J. Non-Cryst. Solids* **2015**, *411*, 137–144. [[CrossRef](#)]
55. Goj, P.; Ciecńska, M.; Szumera, M.; Stoch, P. Thermal properties of Na₂O-P₂O₅-Fe₂O₃ polyphosphate glasses. *J. Therm. Anal.* **2020**, *142*, 203–209. [[CrossRef](#)]
56. Lubas, M.; Sitarz, M.; Fojud, Z.; Jurga, S. Structure of multicomponent SiO₂-Al₂O₃-Fe₂O₃-CaO-MgO glasses for the preparation of fibrous insulating materials. *J. Mol. Struct.* **2005**, *744*, 615–619. [[CrossRef](#)]
57. Öveçoglu, M.L.; Kuban, B.; Özer, H. Characterization and crystallization kinetics of a diopside-based glass-ceramic developed from glass industry raw materials. *J. Eur. Ceram. Soc.* **1997**, *17*, 957–962. [[CrossRef](#)]
58. Cho, Y.S.; Jo, Y.H.; Choi, H.R.; Shin, D.W.; Chung, K.W. Influences of alkali oxides on crystallization and dielectric properties of anorthite-based low temperature dielectrics. *J. Ceram. Soc. Jpn.* **2008**, *116*, 825–828. [[CrossRef](#)]
59. Bayazit, M.; Isik, I.; Cereci, S. FT-IR Spectroscopic Analysis of Potsherds Excavated from The First Settlement Layer of Kuriki Mound. Turkey. In *International Journal of Modern Physics: Conference Series, Proceedings of the International Conference on Ceramics, Bikaner, India, 12–13 December 2012*; World Scientific Publishing Company: Singapore, 2013; Volume 22, pp. 103–111. [[CrossRef](#)]
60. Swamy, V.; Dubrovinsky, L.S.; Tutti, F. High-Temperature Raman Spectra and Thermal Expansion of Wollastonite. *J. Am. Ceram. Soc.* **2005**, *80*, 2237–2247. [[CrossRef](#)]
61. Grelowska, I.; Kosmal, M.; Reben, M.; Pichniarczyk, P.; Sitarz, M.; Olejniczak, Z. Structural and thermal studies of modified silica-strontium-barium glass from CRT. *J. Mol. Struct.* **2016**, *1126*, 265–274. [[CrossRef](#)]
62. Keyvani, N.; Marghussian, V.K.; Rezaie, H.R.; Kord, M. Effect of Al₂O₃ Content on Crystallization Behavior, Microstructure, and Mechanical Properties of SiO₂-Al₂O₃-CaO-MgO Glass-Ceramics. *Int. J. Appl. Ceram. Technol.* **2011**, *8*, 203–213. [[CrossRef](#)]
63. Zhang, S.; Zhang, X.; Liu, W.; Lv, X.; Bai, C.; Wang, L. Relationship between structure and viscosity of CaO-SiO₂-Al₂O₃-MgO-TiO₂ slag. *J. Non-Cryst. Solids* **2014**, *402*, 214–222. [[CrossRef](#)]
64. Li, S.; Liu, Z.; Yin, L.; Kang, J.; Qu, Y.; Liang, X.; Yue, Y. The fiber spinnability and mixed alkaline effect for calcium magnesium aluminosilicate glasses. *J. Non-Cryst. Solids* **2021**, *557*, 120643. [[CrossRef](#)]
65. Kjeldsen, J.; Smedskjaer, M.M.; Potuzak, M.; Yue, Y.Z. Role of elastic deformation in determining the mixed alkaline earth effect of hardness in silicate glasses. *J. Appl. Phys. Lett.* **2015**, *117*, 034903. [[CrossRef](#)]
66. Jha, P.; Singh, K. Effect of Field Strength and Electronegativity of CaO and MgO on Structural and Optical Properties of SiO₂-K₂O-CaO-MgO Glasses. *Silicon* **2015**, *8*, 437–442. [[CrossRef](#)]
67. Montoya-Quesada, E.; Villaquirán-Caicedo, M.A.; Mejía de Gutiérrez, R. New glass-ceramic from ternary-quaternary mixtures based on Colombian industrial wastes: Blast furnace slag, copper slag, fly ash and glass cullet. *Boletín De La Soc. Española De Cerámica Y Vidr.* **2021**, *in press*. [[CrossRef](#)]